Monthly Notices of the ROYAL ASTRONOMICAL SOCIETY

MNRAS **470,** 4048–4060 (2017) doi:10.1093/mnras/stx1534
Advance Access publication 2017 June 17

Single photoionization of the Zn II ion in the photon energy range 17.5–90.0 eV: experiment and theory

G. Hinojosa,[1]★ V. T. Davis,[2] A. M. Covington,[2] J. S. Thompson,[2] A. L. D. Kilcoyne,[3] A. Antillón,[1] E. M. Hernández,[1,4] D. Calabrese,[5] A. Morales-Mori,[1] A. M. Juárez,[1] O. Windelius[6,7] and B. M. McLaughlin[8,9]★

[1] *Universidad Nacional Autónoma de México, Instituto de Ciencias Físicas, AP 48-3, Cuernavaca 62251, Mexico*
[2] *Department of Physics, University of Nevada, Reno, NV 89557-0220, USA*
[3] *The Advanced Light Source, Lawrence Berkeley National Laboratory, Berkeley, CA 94720, USA*
[4] *Universidad Autónoma del Estado de Morelos, Avenida Universidad 1001, Cuernavaca 62209, Mexico*
[5] *Department of Physics, Sierra College, Rocklin, CA 95677, USA*
[6] *Department of Applied Physics, Chalmers University of Technology, SE-41296 Göteborg, Sweden*
[7] *Department of Physics, University of Gothenburg, SE-412 96 Göteborg, Sweden*
[8] *Centre for Theoretical Atomic and Molecular Physics (CTAMOP), School of Mathematics and Physics, Queen's University Belfast, Belfast BT7 1NN, UK*
[9] *Institute for Theoretical Atomic and Molecular Physics (ITAMP), Harvard–Smithsonian Center for Astrophysics, MS-14, Cambridge, MA 02138, USA*

Accepted 2017 June 15. Received 2017 June 12; in original form 2017 May 22

ABSTRACT

Measurements of the single-photoionization cross-section of Cu-like Zn^+ ions are reported in the energy (wavelength) range 17.5 eV (708 Å) to 90 eV (138 Å). The measurements on this *trans*-Fe element were performed at the Advanced Light Source synchrotron radiation facility in Berkeley, California at a photon energy resolution of 17 meV using the photon–ion merged-beams end-station. Below 30 eV, the spectrum is dominated by excitation autoionizing resonance states. The experimental results are compared with large-scale photoionization cross-section calculations performed using a Dirac Coulomb *R*-matrix approximation. Comparisons are made with previous experimental studies, resonance states are identified and contributions from metastable states of Zn^+ are determined.

Key words: atomic data – atomic processes – scattering.

1 INTRODUCTION

About half of the heavy elements ($Z \geq 30$) in the Universe were formed during the asymptotic giant branch phase through slow neutron-capture (*n*-capture) nucleosynthesis (the *s*-process). In the intershell between the H- and He-burning shells, Fe-peak nuclei experience neutron captures interlaced with β-decays, which transform them into heavier elements. For example, in spite of its cosmic rarity, atomic selenium has been detected in the spectra of stars (Roederer 2012; Roederer et al. 2014) and of astrophysical nebulae (Sterling & Dinerstein 2008; Sterling et al. 2009; García-Rojas et al. 2015, 2016). The chemical composition of these objects illuminates details of stellar nucleosynthesis and the chemical evolution of galaxies. To interpret such astrophysical spectra requires three types of fundamental parameters: (i) the energy of internal states (or transition frequencies), (ii) transition probabilities (or Einstein A-coefficients) and (iii) collisional excitation rate coefficients (or collision strengths in the case of electron impact). While these parameters have been studied over the past century for many atomic and molecular species, the necessary information is far from complete or is of insufficient reliability. Extensive data bases do exist for the first two items [e.g. National Institute of Standards and Technology (NIST)], referred to as spectroscopic data; the situation for the last item is far less satisfactory.

However, atomic data, such as PI cross-sections, are unknown for the vast majority of *trans*-Fe, *n*-capture element ions. We note that the *n*-capture elements, Cd, Ge and Rb, were recently detected in planetary nebulae (Sterling et al. 2016). Measurements for the photoionization (PI) cross-section on the *trans-Fe* element Se in various ionized stages (Esteves et al. 2011, 2012; Sterling & Witthoeft 2011; Sterling et al. 2011a,b; Macaluso et al. 2015) provided critically needed data to astrophysical modellers (Sterling & Stancil 2011; Sterling, Porter & Dinerstein 2015; García-Rojas et al. 2016) and were benchmarked against results from a recently developed suite of fully relativistic parallel Dirac Atomic *R*-matrix (DARC) codes (McLaughlin & Ballance 2012a,b, 2015; Ballance 2016; McLaughlin et al. 2016, 2017) achieving excellent agreement.

Studies of Zn I abundance in metal-poor stars are used to infer the histories of galactic chemical evolution. Unfortunately, a major

★ E-mail: hinojosa@icf.unam.mx (GH); bmclaughlin899@btinternet.com (BMM);

source of uncertainty in all these studies is the lack of accurate knowledge of atomic parameters, such as transition wavelengths, cross-sections for PI, electron-impact excitation (EIE), dielectronic recombination and line-strengths (Sneden, Gratton & Crocker 1991; Mishenina et al. 2002; Roederer et al. 2010; Roederer, Marino & Sneden 2011; Frebel, Simon & Kirby 2014).

PI of atomic ions is an important process in determining the ionization balance and the abundances of elements in photoionized astrophysical nebulae. It has recently become possible to detect neutron *n*-capture elements (Se, Cd, Ga, Ge, Rb, Kr, Br, Xe, Ba and Pb) in a large number of ionized nebulae (Sharpee et al. 2007; Sterling, Dinerstein & Kallman 2007; Sterling & Dinerstein 2008). These elements are produced by slow or rapid *n*-capture nucleosynthesis. Measuring the abundances of these elements helps to reveal their dominant production sites in the Universe, as well as details of stellar structure, mixing and nucleosynthesis (Langanke & Wiescher 2001; Sharpee et al. 2007; Sterling et al. 2016). These astrophysical observations are the motivation to determine the EIE, electron-impact ionization, PI and recombination properties of *n*-capture elements (Cardelli et al. 1993; Wallerstein et al. 1997; Busso, Gallino & Wasserburg 1999; Langanke & Wiescher 2001; Travaglio et al. 2004; Herwig 2005; Cowan & Sneden 2006; Smith & Lambert 2015).

The validity of various theories of galactic evolution, stellar nucleosynthesis, the interplay of gravity and chemistry in various stellar bodies all depend on accurate measurements of metals within different types of astrophysical objects such as large stars, nebulae and globular clusters (Sneden et al. 1991; Mishenina et al. 2002; Djeniže, Milosavljevic & Dimitrijevic 2003; Chen, Nissen & Zhao 2004; Nissen et al. 2004, 2007; Chayer et al. 2005; Kobayashi & Nomoto 2009; Hollek et al. 2011; Jose & Iliadis 2011; Roederer et al. 2011; Hinkel et al. 2014). The oldest parts of the Milky Way galaxy are the metal-poor stars in the thick disc. The origin and evolution of the chemical and dynamical structures of the thick disc remain unclear. Chemical abundances in stars of the thick disc and in the inner and outer halo stars are important because the ratios of heavy elements to Fe in these stars can reveal different formation mechanisms. [Zn/Fe] ratios in outer halo stars can be used to distinguish formation time-scales of these stars from those of stars in the disc (Chen et al. 2004; Nissen et al. 2004; Tumlinson 2006).

The relevance that atomic parameters have in astrophysics and in our understanding of the chemical evolution and the chemical assembly of progenitor nebulae is derived from measurements of elemental abundances of zinc. In these nebulae, zinc happens to be a better indicator of Fe and Fe-group abundances, as it does not condense into dust as easily as iron. Some nebulae do not show the abundance of Zn that models predict, indicating that reliable data on this species are of critical importance in the study of these systems (Karakas et al. 2009).

Experimental studies on the PI of ions from intermediate-sized atoms provide a wealth of spectroscopic data and cross-section values. PI cross-section data on *trans*-Fe ions can be used to advance theoretical models in light of details that substantial photon flux and high-energy resolution have the power to reveal. To our knowledge, the only data available on the PI of the *trans*-Fe element, Zn II, is the pioneering experimental work by Peart, Lyon & Dolder (1987), using a merged-beams technique by combining synchrotron radiation (SR) with a beam of Zn^+ at the Daresbury radiation facility. Peart et al. (1987) succeeded in observing several resonances and measured the PI cross-section with moderate photon energy resolution, at the Daresbury beamline (Lyon et al. 1986, 1987; Peart et al. 1987), which had an energy resolution ($\Delta\lambda$) ranging from 0.2 to 1 Å, or approximately 20–4 meV (Lyon et al. 1986). Since the photon flux for measurements on Zn II ions (Peart et al. 1987) was low, a direct measurement of the background PI cross-section was not possible nor was identification of the peaks in the spectrum. The previous work of Peart et al. (1987), however, may be used for comparison purposes and verification of the data presented here.

Previous studies on the PI of Zn I and species iso-electronic to Zn II, relevant to the present work, have been performed by Harrison et al. (1969), who studied PI of the neutral Zn atom, using UV discharge sources. Müller, Schmidt & Zimmermann (1986) studied PI of the iso-electronic neutral Cu atom. From a theoretical point of view, Zn I is the first transition metal with a closed *d*-shell with possible *np* resonances (Stener & Decleva 1997). Apart from its fundamental importance, in astrophysics, PI of Zn^+ (Zn II) is of great practical interest. Recently, Ganeev et al. (2016) demonstrated that autoionizing states of Zn II and Zn III have the ability to enhance harmonics in laser-produced plasmas. We note the K_α X-ray spectrum of the Cu atom has also been measured recently by Mendenhall et al. (2017). Autoionizing states are, in general, excited states with energies that are not commonly studied in the literature. In this work, energies for several of these intermediate autoionizing resonant states have been measured and identified.

The prime motivation for this study of the *trans*-Fe element, Zn II, is to provide benchmark PI cross-section data for applications in astrophysics. High-resolution measurements of the PI cross-section of Zn^+ were performed at the Advanced Light Source (ALS) SR facility in Berkeley, California, over the photon energy range 17.4–90 eV at a resolution of 17 meV FWHM (full width at half-maximum). Several highly excited states have been identified in the energy (wavelength) range 20 eV (620 Å) to 90 eV (138 Å). The high-resolution ALS PI cross-sections are used to benchmark large-scale DARC calculations in this same energy interval. A comparison of the DARC PI cross-sections with previous experimental studies (Peart et al. 1987) and the present ALS work indicates excellent agreement, providing further confidence in the data for various astrophysical applications.

2 EXPERIMENT

The present experimental technique and apparatus have been described in detail previously by Covington et al. (2002). Recent improvements to the technique have been discussed by Müller and collaborators (Müller et al. 2014, 2015). Here, we present a brief description with details relevant to the present measurements. The experimental method is known as the merged-beams technique (Peart, Stevenson & Dolder 1973; Lyon et al. 1986, 1987). The method consists of overlapping trajectories of two beams; in this case, a photon beam from the ALS synchrotron at the Lawrence Berkeley National Laboratory and a counter-propagating ion beam of Zn^+ ions. The experiment was designed to count the resulting Zn^{2+} ions and measure the relevant parameters of the ion and photon beams as well as their spatial overlap.

The photon beam was generated by a 10-cm-period undulator located in the synchrotron ring. The synchrotron was operated under an almost constant electron current of 0.5 A at 1.9 GeV. The resulting photon beam had a maximum width of 1.5 mm and a divergence less than $0.^{\circ}06$. In the grazing incidence mode, the photon beam was directed on to a spherical grating with controls that allowed changes to the photon beam energy to be made as desired.

We used a side-branch gas cell with either He or Kr gases to calibrate the photon energy in the energy range from 18.601 to 92.437 eV (King et al. 1977; Domke et al. 1996). A polynomial fit to reference energy values was used to calibrate the energy scale (along with the Doppler shift correction due to the counter-propagating

photon and ion beams). As a result of the calibration, our data are in agreement with the values reported by NIST (Kramida et al. 2016) to three significant figures. The uncertainty associated with this procedure is estimated to be ±10 meV. The Zn^+ ion beam was produced with an all-permanent magnet electron cyclotron resonance ion source by evaporating zinc in an oven that was inserted into the ion source chamber, with argon used as a support or buffer gas. A 60°-sector analysing magnet was used to separate (as a function of its momentum-to-charge ratio) the Zn^+ cations that had a kinetic energy of 6 keV. A cylindrical Einzel lens, two sets of steering plates and a set of slits were used to focus and collimate the ion beam. A set of electrostatic 90° spherical-sector plates was used to merge the ion beam with the photon beam.

The ions then entered a voltage-biased cylindrical interaction region (IR) and Zn^{2+} photoions produced inside it had a different energy as compared to those produced outside, thereby energy-labelling the ions generated within the specific length of the IR. Energy-tagged Zn^{2+} ions were subsequently separated from the primary Zn^+ ion beam by a 45° dipole analysing magnet.

The experiment was carried out in two different operational modes. The purpose of the first operational mode was to obtain precise knowledge of the interaction length and beam overlap in order to measure the cross-section. In this operational mode, the overlap of the two beams within the IR was carefully measured at discrete photon energies. An absolute-calibrated photodiode was used while operating in this mode.

In the second mode, the photoion signal was maximized without monitoring the actual overlap of the beams within the IR. While running in this mode, the IR voltage was also maintained at all times and the beams overlap was monitored at only some photon energies between successive energy range scans, resulting in a photoion yield spectrum that was later normalized to the absolute measurements. The purpose of measuring spectroscopic energy scans with the IR voltage on was to measure the absolute cross-sections by slightly tuning back the overlap at the pre-established photon energies. Integration times of 200 s were used to account for the stabilization time of the photodiode current reading.

The Zn^+ ion beam was measured by an extended Faraday cup. The resulting Zn^{2+} photoions were counted of the dipole analysing magnet whose magnetic field was adjusted so that only product photoions generated inside the IR were collected. In addition, by using a chopper wheel in the photon beam, the Zn^{2+} signal was background subtracted to remove those ions that were produced by collisions with residual gas in the IR. To derive absolute PI cross-sections, two-dimensional beam profiles of the ion beam $I^+(x, y)$ and the photon beam $I(x, y)$ were measured and used to calculate the interaction volume of the two beams. Three beam translating-slit profilers were used to sample the form factor $F(z)$ according to

$$F(z) = \frac{\int\int I^+(x,y) I^\gamma(x,y)\,\mathrm{d}x\,\mathrm{d}y}{\int I^+(x,y)\,\mathrm{d}x\,\mathrm{d}y \int I^\gamma(x,y)\,\mathrm{d}x\,\mathrm{d}y}, \quad (1)$$

where z is the reference axis assigned to the propagation direction of the ion beam. $F(z)$ was measured at three positions, at the entrance, in the centre and at the exit of the IR. Measured values of these positions were labelled as $i = 1, 2, 3$, respectively. With these three values of $F_i(z)$, $F(z)$ was interpolated within the IR length and integrated over z to compute the spatial overlap of the photon and ion beams along the common IR path.

Absolute cross-section measurements were performed at specific photon energies [open circles (magenta) in Figs 1(a) and (b)] where no resonant structure was present in the spectrum and are tabulated in Table 1. The single-PI cross-section for Zn^+ was derived from the expression

$$\sigma = \frac{Rqe^2 v_i \epsilon}{I^+ I^\gamma \int F(z)\,\mathrm{d}z}, \quad (2)$$

where R is the photoion count rate, $q = 1$ is the charge state of Zn^+, $e = 1.6\times 10^{-19}$ C, v_i is the ion beam velocity in cm s^{-1}, ϵ is the responsivity of the photodiode (electrons per photon), I^+ is the ion beam current (A) and I^γ is the photodiode current (A). In this experiment, the photoion counting efficiency was practically 100 per cent.

The largest sources of systematic error originate from the beam-overlap integral, the beam profile measurements and the photodiode responsivity function. Other contributions to the total systematic error are listed in Covington et al. (2002). All sources of systematic error combine to yield a total uncertainty of 20 per cent, estimated at the 90 per cent confidence level.

The spectra shown in Fig. 1 and in panel (a) of Fig. 2 were measured at 5–10 eV-wide photon energy intervals. Each interval overlapped its neighbouring intervals by 1.0 eV. All the individual parts of the spectra were later combined by joining adjacent regions to produce the entire measured spectrum. An estimation of the photon energy uncertainty caused by this gluing procedure was not greater than ±8 meV.

The overall energy uncertainty propagated by both the gas cell energy calibration and the data reduction procedure is ±13 meV. The photoion yield spectra were normalized by using the measurements at the discrete photon energies of the absolute PI cross-section.

It is important to point out that corrections in the cross-section caused by higher-order radiation in the photon beam (mainly second- and third-order radiation in the lower energy regime) can be significant in this photon beamline. The correction to the cross-section at 20 eV was estimated to be almost 40 per cent by Müller et al. (2015), who derived a correction function f_c for this photon beamline. The error of this correction is 50 per cent of the difference between the uncorrected and the higher-order-corrected cross-section.

Table 2 gives the correction factor f_c to the cross-section due to high-order radiation effects in the photon beam for the present measurements used in our work. Instead of directly applying the correction function of Müller et al. (2015), we used an approximation by interpolating the values of f_c from Müller et al. (2015) listed in Table 2, and included values at 30 and 35 eV. From this approximation, we found that at 17.4 eV the total uncertainty is 33 per cent and at 19.64 eV the total uncertainty is already below 20 per cent. Hence for the present experiment, we quote a total error of 33 per cent below 19.64 eV and 20 per cent for higher energies in the spectrum.

3 THEORY

3.1 Atomic structure

The GRASP code (Dyall et al. 1989; Parpia, Froese-Fisher & Grant 2006; Grant 2007) was used to generate the target wavefunctions employed in our collisions work. All orbitals were physical up to $n = 3$, $4s$ and $4p$. We began by doing an extended averaged level (EAL) calculation for the $n = 3$ orbitals. All EAL calculations were performed on the lowest 24 fine-structure levels of the residual Zn III ion, in order to generate target wavefunctions for our PI studies. In our work, we retained all the 355 levels originating from one- and two-electron promotions from the n

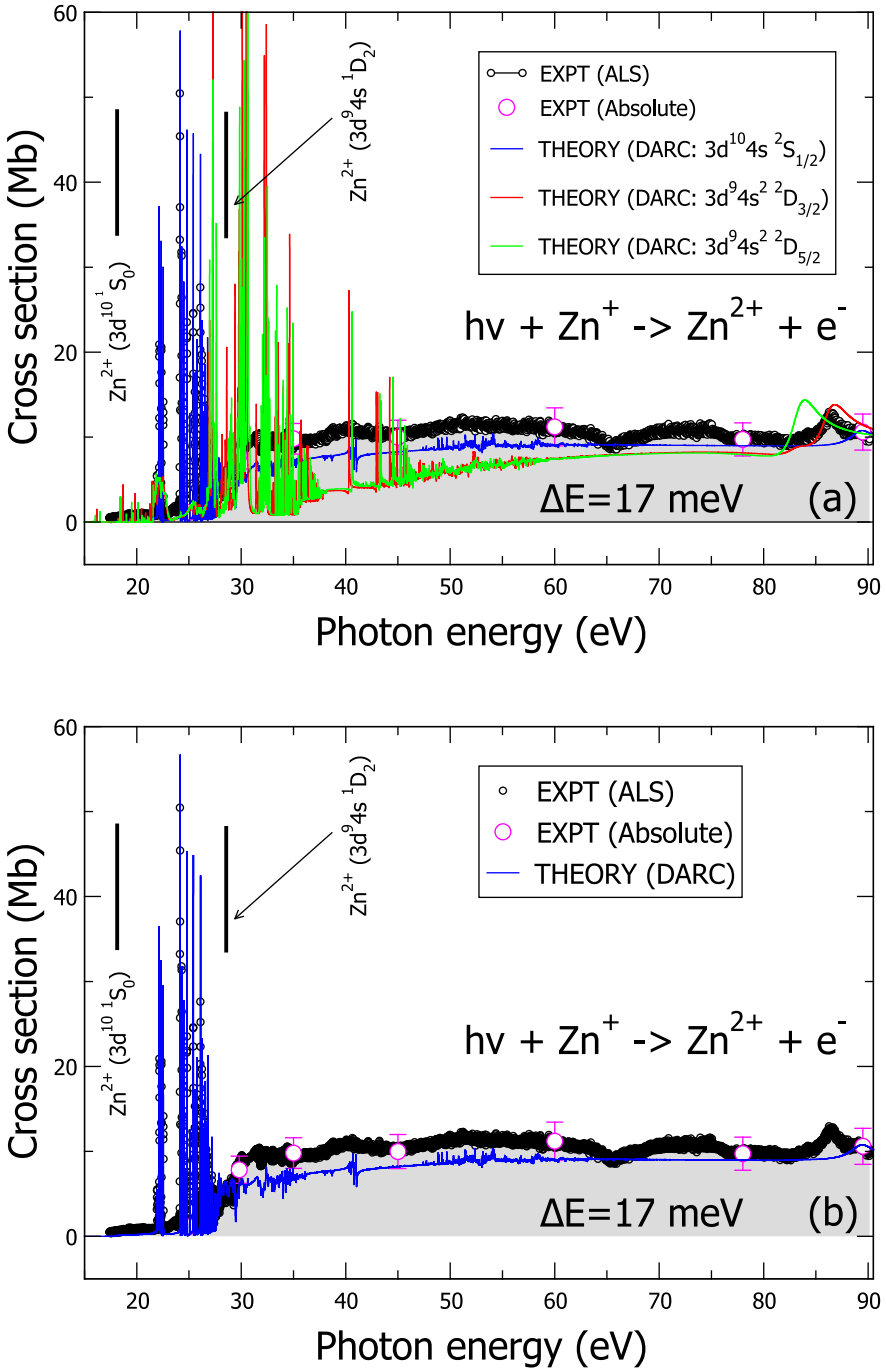

Figure 1. Single-PI cross-section of Zn^+: ALS experimental data (open circles) and the 355-level Dirac *R*-matrix theoretical results. The ALS spectrum consists of Zn^{2+} ion yield spectra normalized to the absolute cross-section measurements (magenta open circles). The thresholds for $Zn^{2+}(3d^{10}\,{}^1S_0)$ at 17.964 eV and $Zn^{2+}(3d^9 4s\,{}^1D_2)$ at 28.317 eV, respectively, are indicated by vertical lines. The correction factor f_c has not been applied to the ALS data illustrated in the figures. (a) ALS measurements and the DARC PI calculations for the ground ($3d^{10}4s^2\,{}^2S_{1/2}$) (blue line) and metastable ($3d^9 4s^2\,{}^2D_{3/2}$ (red line) and $3d^9 4s^2\,{}^2D_{5/2}$) (green line) contributions. (b) ALS measurements and the DARC PI calculations with an appropriate mixture of the ground and metastable states. See text for details.

= 3 levels into the orbital space of this ion. All 355 levels from the 16 configurations were included in the DARC close-coupling calculation, namely: $3s^2 3p^6 3d^{10}$, $3s^2 3p^6 3d^9 4s$, $3s^2 3p^6 3d^9 4p$, $3s^2 3p^5 3d^{10} 4s$, $3s^2 3p^5 3d^{10} 4p$, $3s 3p^6 3d^{10} 4s$, $3s 3p^6 3d^{10} 4p$, $3s^2 3p^6 3d^8 4s^2$, $3s^2 3p^6 3d^8 4p^2$, $3s^2 3p^6 3d^8 4s 4p$, $3s^2 3p^4 3d^{10} 4s^2$, $3s^2 3p^4 3d^{10} 4p^2$, $3s^2 3p^4 3d^{10} 4s 4p$, $3p^6 3d^{10} 4s^2$, $3p^6 3d^{10} 4p^2$ and $3p^6 3d^{10} 4s 4p$.

Table 3 gives a sample of the theoretical energy levels from the 355-level GRASP calculations for the lowest 17 levels of the residual Zn^{2+} ion, compared to the values available from the NIST tabulations (Kramida et al. 2016). The average percentage difference of our theoretical energy levels compared with the NIST values is approximately 12 per cent. For the $3d^{10}\,{}^1S_0 \rightarrow 3d^9 4p\,{}^3P^o_1$ transition, we obtained a value of 4.0×10^{-3} for the oscillator strength

Table 1. Zn^+ absolute single-PI valence shell cross-section made at the ALS with a 17 ± 3 meV photon energy resolution in the photon energy range 25–90 eV.

Energy (eV)	σ (Mb)
25.0	1.14 ± 0.23
29.8	7.83 ± 1.60
35.0	9.80 ± 1.80
45.0	9.99 ± 2.00
60.0	11.20 ± 2.24
78.0	9.73 ± 1.95
89.5	10.60 ± 2.14

(*f*-value). This is to be compared with the *f*-value of 5.0×10^{-3}, for the same transition from the MCDF work of Yu et al. (2007). From our GRASP calculations, we obtained values of 1.3 *ns* and 1.8 *ns* for the radiative lifetimes for the 1581 and 1673 Å lines, respectively, the $3d^9 4p\ ^3F^o_4 \rightarrow 3d^9 4s\ ^3D_3$ and $3d^9 4p\ ^3P^o_2 \rightarrow 3d^9 4s\ ^3D_3$ transitions in Zn III. Our values are in respectable agreement with the experimental results of 1.1 ± 0.3 *ns* and 1.2 ± 0.3 *ns* from the previous work of Andersen, Pedersen & Biemont (1997).

PI cross-sections were then performed on the Zn II ion for the $3d^{10}4s\ ^2S_{1/2}$ ground state and the $3d^9 4s^2\ ^2D_{3/2,5/2}$ metastable levels using the DARC codes, with these Zn III residual ion target wavefunctions.

3.2 Photoionization calculations

For comparison with high-resolution measurements made at the ALS, state-of-the-art theoretical methods with highly correlated wavefunctions that include relativistic effects are used. The scattering calculations were performed for PI cross-sections using the above large-scale configuration interaction target wavefunctions as input to the parallel DARC suite of *R*-matrix codes.

The General Relativistic Atomic Structure Package (GRASP; Dyall et al. 1989; Grant 2007) formulates and diagonalizes a Dirac-Coulomb Hamiltonian (Grant 2007) to produce the relativistic orbitals for input to the DARC (Chang 1975; Norrington & Grant 1981; Grant 2007; Burke 2011) to obtain the PI cross-sections. These DARC codes are currently running efficiently on a variety of world-wide parallel High Performance Computer (HPC) architectures (McLaughlin & Ballance 2015; McLaughlin et al. 2015, 2016, 2017; Ballance 2016).

15 continuum orbitals were used in our scattering calculations. A boundary radius of 9.61 a_0 was necessary to accommodate the diffuse $n = 4$ bound state orbitals of the residual Zn III ion. To fully resolve the resonance features present in the spectrum, an energy grid of $2.5 \times 10^{-7}\ \mathcal{Z}^2$ Ry (13.6 μeV), where $\mathcal{Z} = 2$, was utilized in our collision work.

PI cross-section calculations with this 355-level model were then performed with this fine energy mesh for the $3d^{10}4s\ ^2S_{1/2}$ ground state and the $3d^9 4s^2\ ^2D_{5/2,\,3/2}$ metastable levels of this ion, over the photon energy range similar to experimental studies. This ensured that all the fine resonance features were fully resolved in the respective PI cross-sections.

For the $^2S_{1/2}$ level, we require the bound-free dipole matrices, $J^\pi = 1/2^e, \rightarrow J'^{\pi'} = 1/2^o$ and $3/2^o$. In the case of the $^2D_{5/2,\,3/2}$ metastable levels, we required the $J^\pi = 3/2^e, \rightarrow J'^{\pi'} = 1/2^o, 3/2^o, 5/2^o$ and the $J^\pi = 5/2^e, \rightarrow J'^{\pi'} = 3/2^o, 5/2^o, 7/2^o$ bound-free dipole matrices. The *jj*-coupled Hamiltonian diagonal matrices were adjusted so that the theoretical term energies matched the recommended experimental values of the NIST tabulations (Kramida et al. 2016). We note that this energy adjustment ensures better positioning of resonances relative to all thresholds included in the present calculations.

3.3 Resonances

The energy levels available from the NIST tabulations (Kramida et al. 2016) were used as a helpful guide for the present assignments. The resonance series identification can be made from Rydberg's formula (Rydberg 1890, 1893, 1894; Eisberg & Resnik 1985):

$$\epsilon_n = \epsilon_\infty - \frac{\mathcal{Z}^2}{\nu^2}, \tag{3}$$

where Rydbergs ϵ_n is the transition energy and ϵ_∞ is the ionization potential of the excited electron to the corresponding final state ($n = \infty$), i.e. the resonance series limit with n being the principal quantum number. The relationship between the principal quantum number n, the effective quantum number ν and the quantum defect μ for an ion of effective charge $\mathcal{Z}$ is given by $\nu = n - \mu$ (Shore 1967; Seaton 1983). Converting all quantities to eV, we can represent the Rydberg series as

$$E_n = E_\infty - \frac{\mathcal{Z}^2 \mathcal{R}}{(n-\mu)^2}. \tag{4}$$

Here, E_n is the resonance energy, E_∞ is the resonance series limit, $\mathcal{Z}$ is the charge of the core (in this case $\mathcal{Z} = 2$) and μ is the quantum defect ($\mu_{ns} > \mu_{np} > \mu_{nd} > \mu_{nf}, \ldots$), with μ being zero for a pure hydrogenic state. For a hydrogenic system, this can be written as

$$E_n^{\rm H} = E_\infty - \frac{\mathcal{Z}^2 \mathcal{R}}{n^2}, \tag{5}$$

where the Rydberg constant $\mathcal{R}$ is $R_\infty = 13.605\,698$ eV.

The multichannel *R*-matrix eigenphase derivative (QB) technique, which is applicable to atomic and molecular complexes, as developed by Berrington and co-workers (Quigley & Berrington 1996; Quigley, Berrington & Pelan 1998; Ballance, Berrington & McLaughlin 1999), was used to locate and determine the resonance positions. The resonance width Γ may also be determined from the inverse of the energy derivative of the eigenphase sum δ at the resonance energy E_r via

$$\Gamma = 2\left[\frac{{\rm d}\delta}{{\rm d}E}\right]^{-1}_{E=E_r} = 2\left[\delta'\right]^{-1}_{E=E_r}. \tag{6}$$

4 RESULTS AND DISCUSSION

The ALS spectrum for the single PI of Zn^+ cross-section measurements is illustrated in Figs 1(a) and (b), along with the absolute measurements and the results from the large-scale DARC PI cross-section calculations. The ALS measurements were made in the photon energy range 17.5–90.0 eV with a photon energy resolution of 17 meV. In order to compare directly with experiment, the DARC results have been convoluted with a Gaussian having a profile width of 17 meV. PI calculations were performed for the ground state $3d^{10}4s\ ^2S_{1/2}$ and the $3d^9 4s^2\ ^2D_{3/2,\,5/2}$ metastable states. The absolute PI cross-section measurements are shown in Figs 1(a) and (b) with open circles. Note that the correction factor f_c has not been applied to the ALS measurements. The DARC PI calculations are included in Fig. 1(a) for 100 per cent population of both the ground and metastable states. Fig. 1(b) shows a comparison of the DARC PI cross-section, convoluted using a Gaussian having a profile of

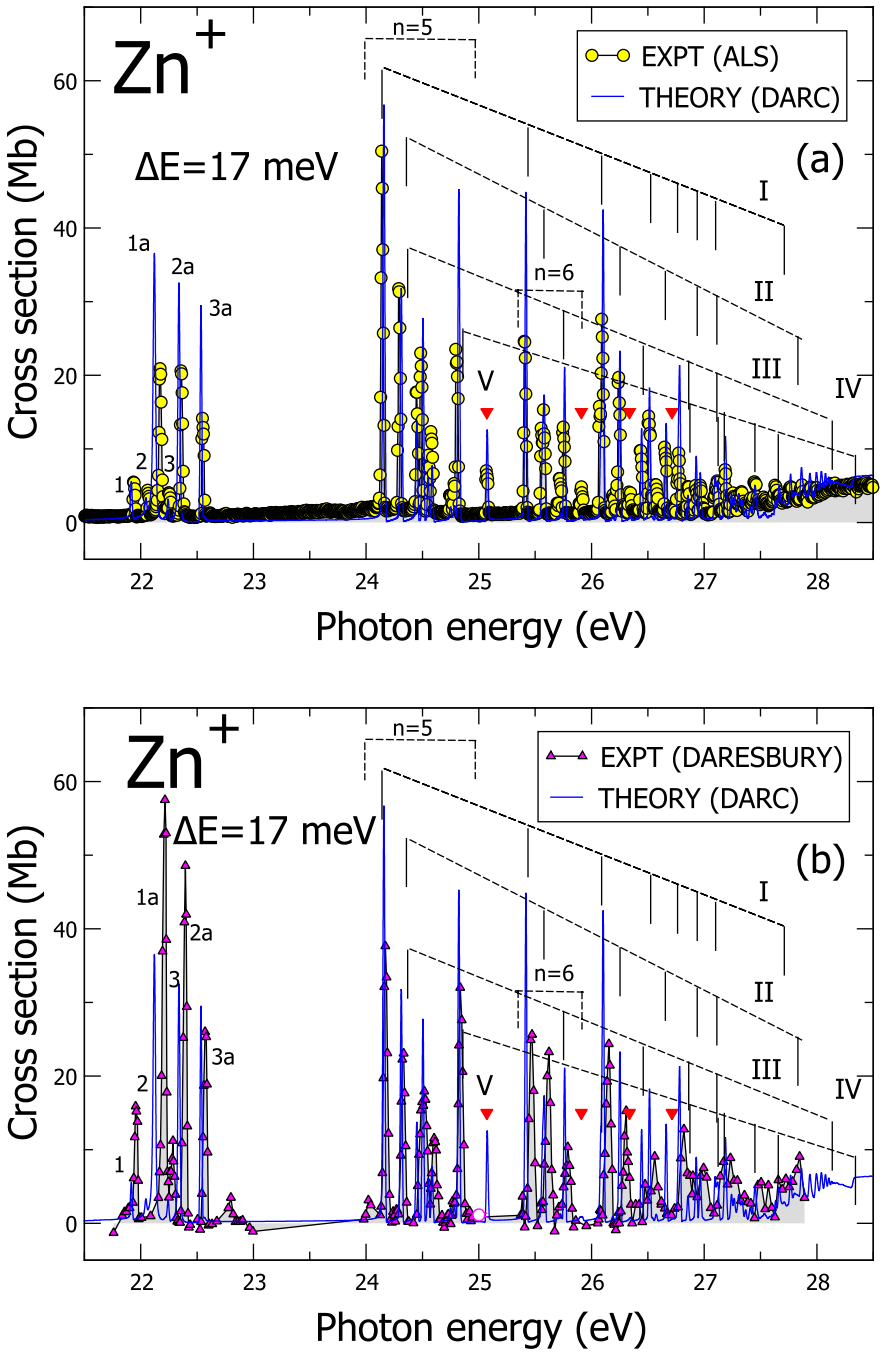

Figure 2. Single-photon, single-PI cross-section of Zn^+: resonance features in the spectrum for 21.5–28.5 eV. (a) ALS measurements are shown by solid circles (yellow), resolution of 17 meV FWHM. (b) DARESBURY are shown by solid triangles (yellow; Peart et al. 1987). In both panels, the large-scale DARC calculations shown by solid line (blue) are convoluted with a Gaussian, having a profile of 17 meV FWHM, with an appropriate admixture of ground and metastable states, see the text for details. Vertical lines indicate the resonant energies of Table 4. The final vertical lines to the right of each group correspond to the limit of the series. Gaussian fits to the peak centres are presented in Tables 4 and 5. The grouped lines of the Rydberg series and vertical lines from panel (a) for those resonances that can be paired with a peak in the data by Peart et al. (1987). Open circle (magenta) indicates the ALS absolute cross-section at 25 eV.

17 meV and an appropriate weighted admixture of 98 per cent ground and 2 per cent of the statistical average of the metastable states, with the ALS measurements. Excellent agreement is obtained between theory and experiment over the energy region investigated.

A restricted region of the spectrum, for the photon energy range 21.5–28.5 eV, is displayed in Figs 2(a) and (b). Fig. 2(a) shows the present ALS spectrum recorded at 17 meV FWHM compared to the DARC calculations. In Fig. 2(b), the previous Zn II digitized spectra obtained at the Daresbury radiation facility (Peart et al. 1987) are illustrated for the same energy region with a similar comparison made with the DARC calculations. In Figs 2(a) and (b), numerous sharp peak structures are seen in the Zn II spectrum over this energy region. The peaks in the spectrum can be assigned to well-defined Rydberg series originating from the ground state, namely, $Zn^+(3d^{10}4s\,^2S_{1/2})$ resonances, converging to the triplet state $3d^9 4s\,^3D_{3,2,1}$ thresholds [i.e. series I, II and III in panel (a) of

Table 2. The correction factor f_c applied to the present measured ALS cross-section data due to the presence of high-order radiation effects in the photon beam. In our work, we interpolated the values from Müller et al. (2015) and included values at 30 and 35 eV.

Photon energy (eV)	Correction factor f_c
16	1.90[a]
20	1.40[a]
25	1.17[a]
30	1.07[b]
35	1.00[b]

[a]Values determined by Müller et al. (2015).
[b]Present values.

Table 3. Zn^{2+} energy levels in Rydbergs (Ry) from the large-scale GRASP calculations compared with the available tabulations from the NIST data base (Kramida et al. 2016). A sample of the lowest 17 levels for the residual Zn^{2+} ion from the 355-level GRASP calculations is shown compared to experiment. The percentage difference Δ(per cent) of individual energy levels is given for completeness.

Level	STATE	TERM	NIST (Ry)	GRASP (Ry)	Δ(per cent)[a]
1	$3d^{10}$	$^1S_0$	0.000 000	0.000 000	0.0
2	$3d^9 4s$	$^3D_3$	0.711 666	0.820 402	15.3
3	$3d^9 4s$	$^3D_2$	0.722 394	0.834 832	15.6
4	$3d^9 4s$	$^3D_1$	0.736 761	0.851 328	15.6
5	$3d^9 4s$	$^1D_2$	0.760 911	0.893 474	17.4
6	$3d^9 4p$	$^3P^o_2$	1.256 331	1.361 426	8.4
7	$3d^9 4p$	$^3P^o_1$	1.276 421	1.385 355	8.5
8	$3d^9 4p$	$^3P^o_0$	1.288 463	1.399 012	8.6
9	$3d^9 4p$	$^3F^o_3$	1.281 741	1.410 420	10.0
10	$3d^9 4p$	$^3F^o_4$	1.287 866	1.411 489	9.6
11	$3d^9 4p$	$^3F^o_2$	1.298 403	1.427 982	10.0
12	$3d^9 4p$	$^1F^o_3$	1.316 792	1.457 057	10.7
13	$3d^9 4p$	$^1D^o_2$	1.323 560	1.468 436	10.9
14	$3d^9 4p$	$^3D^o_3$	1.330 146	1.472 693	10.7
15	$3d^9 4p$	$^3D^o_1$	1.344 768	1.491 643	11.0
16	$3d^9 4p$	$^3D^o_2$	1.347 960	1.496 767	11.0
17	$3d^9 4p$	$^1P^o_1$	1.344 106	1.527 372	13.6

[a]Average Δ(per cent) of the energy levels with experiment is ≈12 per cent.

Fig. 2], and to the singlet state threshold $3d^9 4s\ ^1D_2$ (series IV) of the Zn^{2+} ion.

Series identification was guided by fitting equation (4) to a particular set of peak positions that corresponded to a well-defined series. The Rydberg series limits E_∞ were determined by fitting the series with equation (4), which agreed with results from the tabulations in the NIST data base (Kramida et al. 2016) to three significant figures. Due to several overlapping peaks, values for the resonance energies were derived from Gaussian fits to the peaks to obtain more precise values for the peak centroids. These centroids are presented in Table 4 together with the averaged quantum defects μ_f and the corresponding series limits for the identified Rydberg resonance series.

In the resonant region of the spectrum 24–28 eV, it is seen that there are many interloping and overlapping resonances present. For some of the peaks, their resonance energies in Table 4 are given in parenthesis (or brackets) in order to indicate that they are estimates.

A resonance series with $n \geq 6$, labelled as series V in panel (a) of Fig. 2 (having small strengths), with the same series energy limit $E_\infty = 27.647$ eV of series I, can be identified in the experimental spectrum. Excitation energies were calculated using the Cowan code (Cowan 1981; Mann 1983; Clark, Abdallah & Mann 1991). To compare them with the measured resonance energies E_n (see Fig. 3), a linear fit was used where

$$E_n = m\ E_{\rm Cowan} + b \tag{7}$$

with m and b constants (Müller et al. 2014). This function fitted the measured resonance energies very well for the excited state $E_{\rm Cowan}$ resonance energies.

Below 23 eV, a group of well-resolved resonances is observed, as indicated in panel (a) of Fig. 2. Higher order radiation in the photon beam appears in the low-energy interval of the first grating of the photon beamline, which may result in excitation of the Zn^+ energy levels accessible at higher photon energies. If this is the case, one would expect resonances to also appear at two or three times their photon energies. Since no such peaks were observed [see Figs 1(a) and (b)] at the corresponding higher photon energies, one may conclude that higher order photons are not the source of this particular set of resonances.

In panel (b) of Fig. 2, the earlier findings of Peart et al. (1987) are illustrated along with the DARC results. In this figure, as a guide, we have retained some of the grouping lines, labels, and a single absolute cross-section data point from panel (a) of Fig. 2. The peaks reported by Peart et al. (1987) appear shifted towards higher energies, or shorter wavelengths, compared to the present ALS measurements and the DARC calculations. Differences are seen ranging from about 20 meV (in the lower energy regime) to 60 meV (in the higher energy regime) with their experiment. These differences we attribute to the energy calibration uncertainties reported by Lyon et al. (1986) of 30 meV to 77 meV, in the respective energy regimes. We note also that the DARC peak energies favour the ALS measurements as can be seen from Figs 2(a), (b) and the results tabulated in Table 5.

The peaks in the Zn II spectrum were identified from a theoretical analysis of the eigenphase sum δ and its derivative δ' for the $J = 1/2$ and $J = 3/2$ odd scattering symmetries obtained from the large-scale DARC calculations. The results are presented in Figs 3(a) and (b). We find that the peaks below 23 eV originate from PI of the ground state term and attribute them to excited resonance states $[3d^9 4s\,(^{1,\,3}D_{3,\,2,\,1})\,4p]_{1/2,\,3/2}$ converging to different Zn^{2+} core states. These are labelled 1a–3a and 1–3 in the experimental spectrum. We can assign the remaining peaks to well-defined Rydberg resonance series. We note that the $3d^9 4s\,(^3D_3)\,5p$ resonance, identified with series I, located at 24.141 eV, is the strongest in the spectrum.

An important feature of the spectrum of Figs 1(a) and (b) is the small non-zero cross-section below the ionization threshold (marked by the vertical line). This shift is probably due to the presence of higher order radiation in the photon beam that causes a contribution from the non-resonant cross-section or from the metastable contamination of the ion beam.

To determine the metastable contaminant in the ion beam, large-scale DARC PI calculations were performed for the $3d^9 4s^2\ ^2D_{3/2,\,5/2}$ initial metastable states. From these DARC PI cross-section calculations, we determined that the metastable contamination of the ion beam was 2 per cent by using a statistical average of the metastable theoretical cross-sections compared to the ALS measurements at 17.5 eV. Hence, we conclude that the resonance features in the spectrum originate from the ground state. Fig. 1(a)

Table 4. Resonance energies E_n of the identified Rydberg series I, II, III, IV and V (from the present experimental ALS data) converging to the $3d^9 4s\,{}^3\mathrm{D}_{3,\,2,\,1}$ triplet and the $3d^9 4s\,{}^1\mathrm{D}_2$ singlet states originating from the Zn^+ ground state. Some energies, in brackets, have the same superscript to indicate that they superimpose. In some cases, multipeak Gaussian fits were used to improve assignments when possible. Roman number labels correspond to those of Fig. 2. The average value of the quantum defect μ_f for the Rydberg series corresponds to the value of μ derived from direct fitting to equation (4). Values in parenthesis or brackets are estimates from the fits.

	Autoionizing Zn II Rydberg resonance series energies				
	I	II	III	IV	V
	$(3d^9 4s)^3\mathrm{D}_3\,np$	$(3d^9 4s)^3\mathrm{D}_2\,np$	$(3d^9 4s)^3\mathrm{D}_1\,np$	$(3d^9 4s)^1\mathrm{D}_2\,np$	$(3d^9 4s)^3\mathrm{D}_3\,np$
n	E_n(eV)	E_n(eV)	E_n(eV)	E_n(eV)	E_n(eV)
5	24.141	24.294	24.488	24.804	–
6	25.408	25.569	25.752	[26.069][1]	25.071
7	[26.093][1]	26.243	26.439	[26.773][2]	25.910
8	26.512	26.656	26.858	[27.184][4]	(26.340)
9	[26.773][2]	26.926	[27.116][3]	27.450	(26.714)
10	26.966	[27.104][3]	–	27.632	–
11	[27.087][3]	–	–	27.767	–
12	[27.184][4]	–	–	27.863	–
13	(27.253)	–	–	27.939	–
14	–	–	–	27.994	–
15	–	–	–	28.041	–
⋮					
Limit	27.647	27.793	27.989	28.317	27.647
μ_f	1.11 ± 0.2	1.08 ± 0.2	1.07 ± 0.2	1.05 ± 0.2	1.43 ± 0.3

shows the ALS measurements and the DARC PI calculations for the ground and metastable states, where 100 per cent population of the ground and metastable states are assumed. In Fig. 1(b), the DARC PI calculations have been appropriately weighted, 98 per cent ground state and 2 per cent of the statistical average of the metastable states. As can be seen from the results presented in Figs 1(a) and (b), there is excellent agreement between experiment and theory.

We note that in some cases, the populations of excited states in the ion beams have been estimated to be relatively low (Müller et al. 2014). For example, in a similar ion source, for C-like ions, using the MCDF method, the population of the $^5\mathrm{S}_2$ level was estimated to be 2–3 per cent (Bizau et al. 2005). In this work by performing PI calculations for the metastable states indicated above, we find that their contribution is small, around 2 per cent.

The prominent Rydberg resonance series are identified as $Zn^+(3d^9 4s\,np)$ excitations, as indicated by the series labelled I, II, III and IV in panel (a) of Fig. 2. Resonance energies E_n of each Rydberg resonance series found in the ALS spectrum are tabulated in Table 4 along with the averaged quantum defect μ_f for each series. A $Zn^+(3d^9 4s\,np)$, $n \geq 6$, Rydberg resonance series, as indicated by the downward pointing solid triangles (red), see Figs 2(a) and (b), was also identified in the spectrum. The widths of many of these resonances found in the spectrum, as illustrated in Figs 4(a) and (b), are 10 meV or less making it impossible to extract values with the present limited experimental resolution of 17 meV. The quantum defects μ_n, as a function of the principal quantum number n, for the dominant series are illustrated for the five series, I, II . . . , V, in Fig. 5. Tables 6 and 7 list the resonance energies for these series determined from the QB method.

An additional check on the theoretical data was carried out by comparing the integrated continuum oscillator strength f with experiment. The integrated continuum oscillator strength f of the experimental spectra was calculated over the energy grid $[E_1, E_2]$, where E_1 is the minimum experimental energy and E_2 is the maximum experimental energy measured, (respectively, 17.409 and 91.142 eV), using (Shore 1967; Fano & Cooper 1968; Berkowitz 1979)

$$f = 9.1075 \times 10^{-3} \int_{E_1}^{E_2} \sigma(h\nu)\,\mathrm{d}h\nu$$
$$= 9.1075 \times 10^{-3}\ \overline{\sigma}_{\mathrm{PI}},$$

where

$$\overline{\sigma}_{\mathrm{PI}} = \int_{E_1}^{E_2} \sigma(h\nu)\,\mathrm{d}h\nu \qquad (8)$$

is the resonance strength. Evaluating the continuum oscillator strength f for the ALS cross-section measurements yielded a value of 5.743 ± 1.150, assuming an error of 20 per cent. A similar procedure for the theoretical Dirac R-matrix cross-sections gave a value of 4.966 for 98 per cent of the $3d^{10}4s^2\,{}^1\mathrm{S}_{1/2}$ ground state and 2 per cent of the statistical average of the $3d^9 4s^2\,{}^2\mathrm{D}_{3/2}$ and $3d^9 4s^2\,{}^2\mathrm{D}_{5/2}$ metastable states, in good agreement with experiment. We note that for an individual resonance strength $\overline{\sigma}_{\mathrm{PI}}$, the energy grid $[E_1, E_2]$ is over only the energy span of the resonance. We have used this procedure to determine the resonance strengths from our work.

For the peaks that are well resolved, in the Peart et al. (1987) data, resonance strengths have been derived and are compared with values obtained from the ALS measurements and the DARC calculations. The results are tabulated in Table 5. In general, the resonance strengths of Peart et al. (1987) are much larger than the corresponding values determined from our work. It is seen that only two resonant peaks (with comparable values) are within the uncertainties of both measurements, that is, the two first peaks of group $n = 5$.

It is important to point out that Peart et al. (1987) used an electron bombardment ion source of zinc vapour to generate their Zn^+ ion beam. In a study of emission cross-sections for EIE of Zn^+,

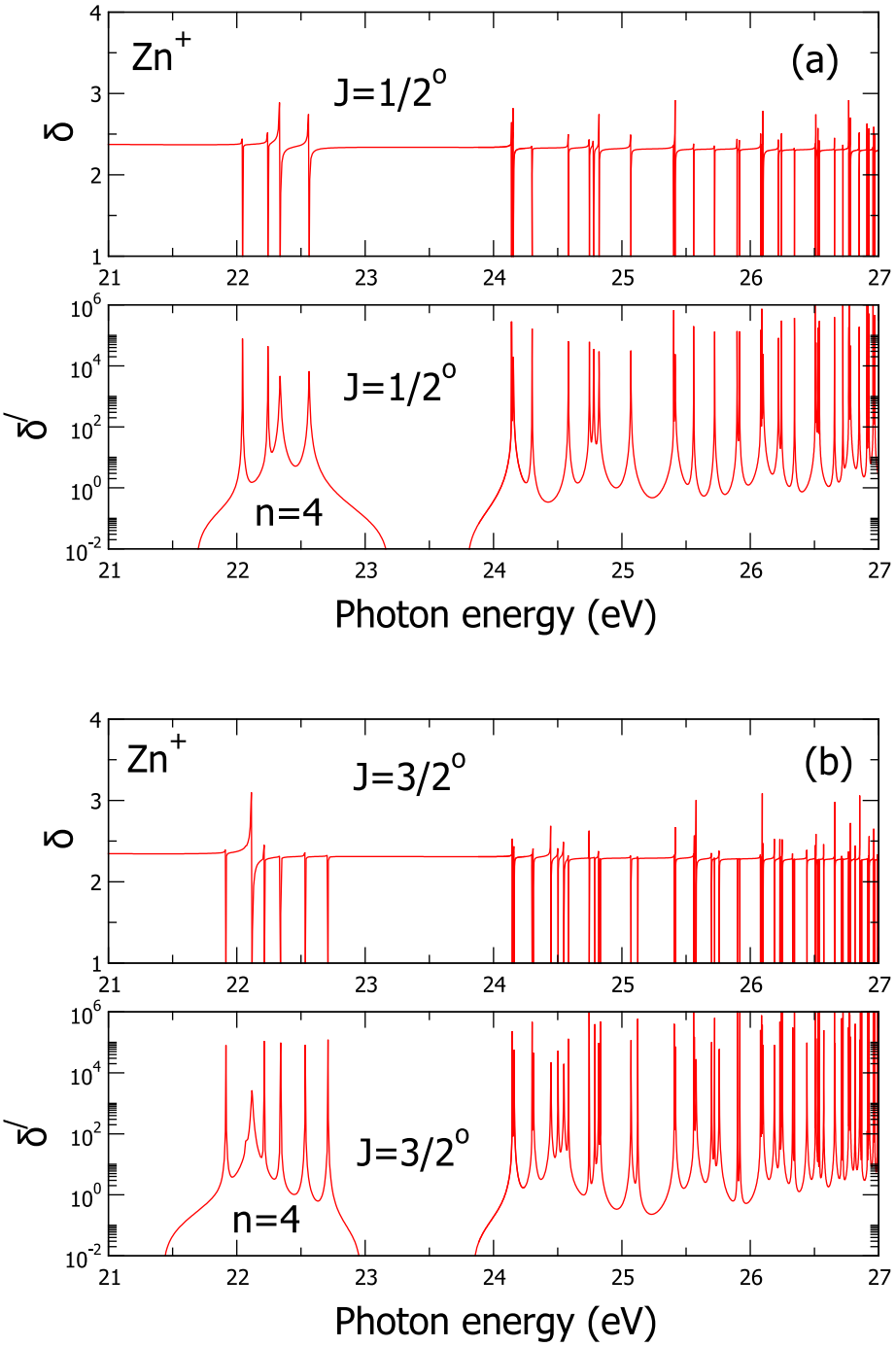

Figure 3. Eigenphase sum δ and its derivative δ' in the photon energy region 21–27 eV for (a) $J = 1/2$ odd scattering symmetry, (b) $J = 3/2$ odd scattering symmetry from the large-scale DARC PI calculations on the Zn II ion. Interloping and overlapping resonances series in the Zn II spectrum disrupt the regular Rydberg resonance series pattern. Tables 6 and 7 give assignments of resonances for each scattering symmetry.

Rogers et al. (1982) used the same type of hot-filament ion source with vapourized zinc metal. They found a large background signal due to higher lying metastable Zn^+ ions in their beam. Metastable contamination in the Zn^+ ion beam was lowered by reducing the ion–source anode voltage to 12 V. Peart et al. (1987) studied the effect on the population of electronic excitation in their ion source by changing the voltage of the anode of their ion source. In this type of ion source, the amount of electronic excitation can be controlled by changing the anode voltage, since at low pressures, this voltage corresponds to the electron impact kinetic energy. In studies of emission cross-sections for EIE of Zn^+ ions, Rogers et al. (1982) showed a difference of less than 20 per cent in the excitation cross-section between the voltages that Peart et al. (1987) used in their comparison (13.4 V and 23.0 V).

This relatively small change in the EIE cross-section of Zn^+ for the two electron kinetic energies, combined with a substantial

Table 5. Resonance energies (E_n) and strengths ($\overline{\sigma}_{\rm PI}$) from the ALS data only for those peaks resolved in the DARESBURY data of Peart et al. (1987) where a comparison is possible. The resonance strengths $\overline{\sigma}_{\rm PI}$ derived from the present ALS data have been multiplied by f_c. Resonance strengths and positions were determined from the large-scale 355-level DARC calculations, assuming 100 per cent of the ground state. The resonance positions for the DARC values were estimated by fitting the peaks in the total cross-sections to Fano profiles. Values in brackets shown (98 per cent of the ground state) are corrected for metastable contamination in the ion beam, determined to be 2 per cent, see text for details.

Resonance	ALS[a]		DARESBURY[b]		DARC[c]	
	E_n	$\overline{\sigma}_{\rm PI}$	E_n	$\overline{\sigma}_{\rm PI}$	E_n	$\overline{\sigma}_{\rm PI}$
label	(eV)	(Mb eV)	(eV)	(Mb eV)	(eV)	(Mb eV)
$n = 4$						
1 ($J = 3/2$)	21.940	0.19 ± 0.05	21.958	0.55	21.919	0.19 (0.18)
1a ($J = 3/2$)	22.173	0.87 ± 0.21	22.210	2.50	22.123	1.22 (1.20)
2a ($J = 1/2$)	22.361	0.69 ± 0.20	22.393	1.70	22.340	0.72 (0.71)
3a ($J = 3/2$)	22.552	0.42 ± 0.13	22.573	0.98	22.535	0.45 (0.44)
$n = 5$	24.141	1.52 ± 0.50	24.172	1.60	24.158	1.42 (1.39)
	24.294	0.99 ± 0.31	24.329	0.98	24.312	0.83 (0.81)
	24.488	0.64 ± 0.23	24.509	1.36	24.504	0.53 (0.52)
	24.804	0.84 ± 0.24	24.839	1.57	25.824	0.97 (0.95)
$n = 6$	25.408	0.77 ± 0.25	25.468	1.34	25.418	1.04 (1.02)
	25.569	0.75 ± 0.15	25.616	1.24	25.577	0.64 (0.63)
	25.752	0.35 ± 0.13	25.786	0.70	25.762	0.41 (0.40)
$n = 7$	(26.093)	(1.13 ± 0.28)	26.150	1.28	26.102	1.32 (1.29)
	26.243	0.62 ± 0.20	26.305	0.77	26.251	0.65 (0.84)

[a] ALS, present experiment.
[b] DARESBURY, previous experimental results (Peart et al. 1987).
[c] DARC, present theory, 355-level approximation.

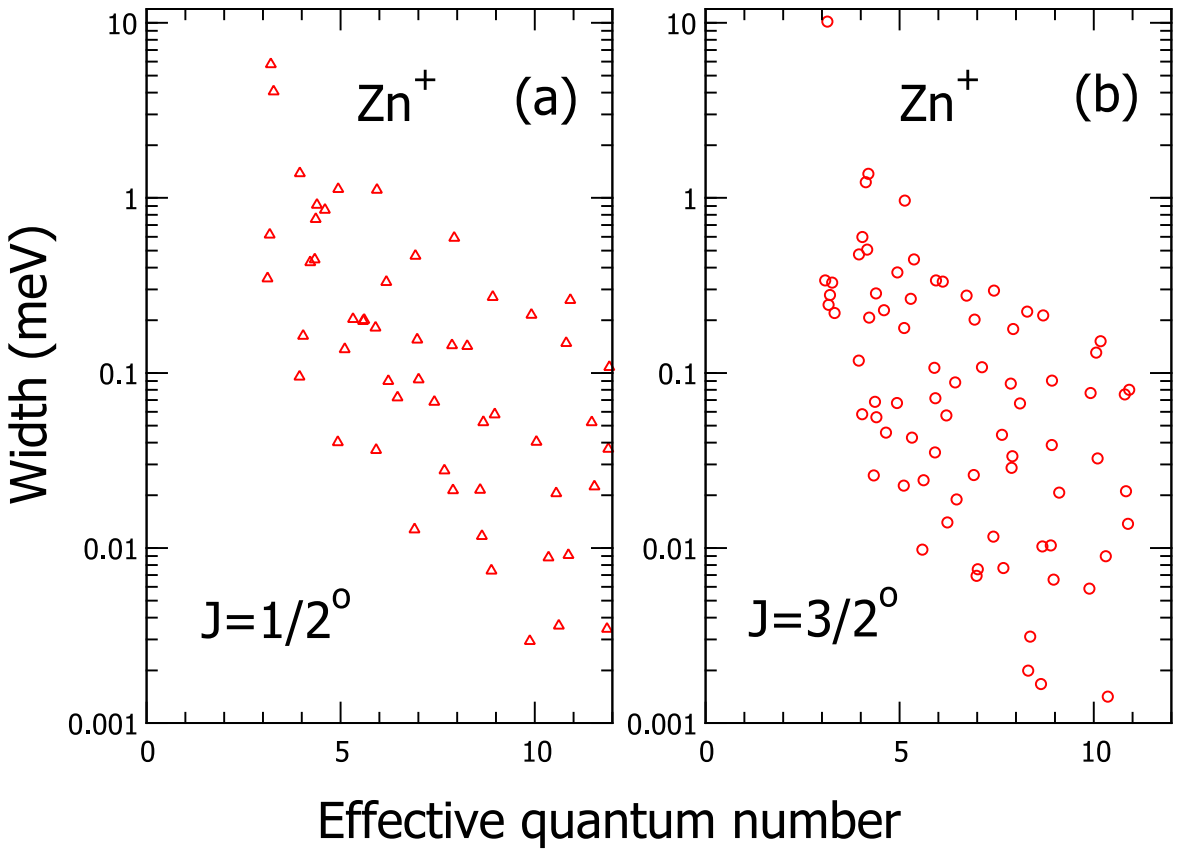

Figure 4. Resonance line widths Γ (meV) versus the effective quantum number ν for resonances series found in the Zn II ALS spectrum in the photon energy range 21–27 eV. (a) $J = 1/2$ odd symmetry and (b) $J = 3/2$ odd symmetry. The theoretical values were obtained using the eigenphase derivative method (Quigley & Berrington 1996; Quigley et al. 1998; Ballance et al. 1999) from the large-scale DARC calculations on the Zn II ion. The resonances line widths are 10 meV or much less and impossible to be extracted with the present limited photon resolution of 17 meV FWHM.

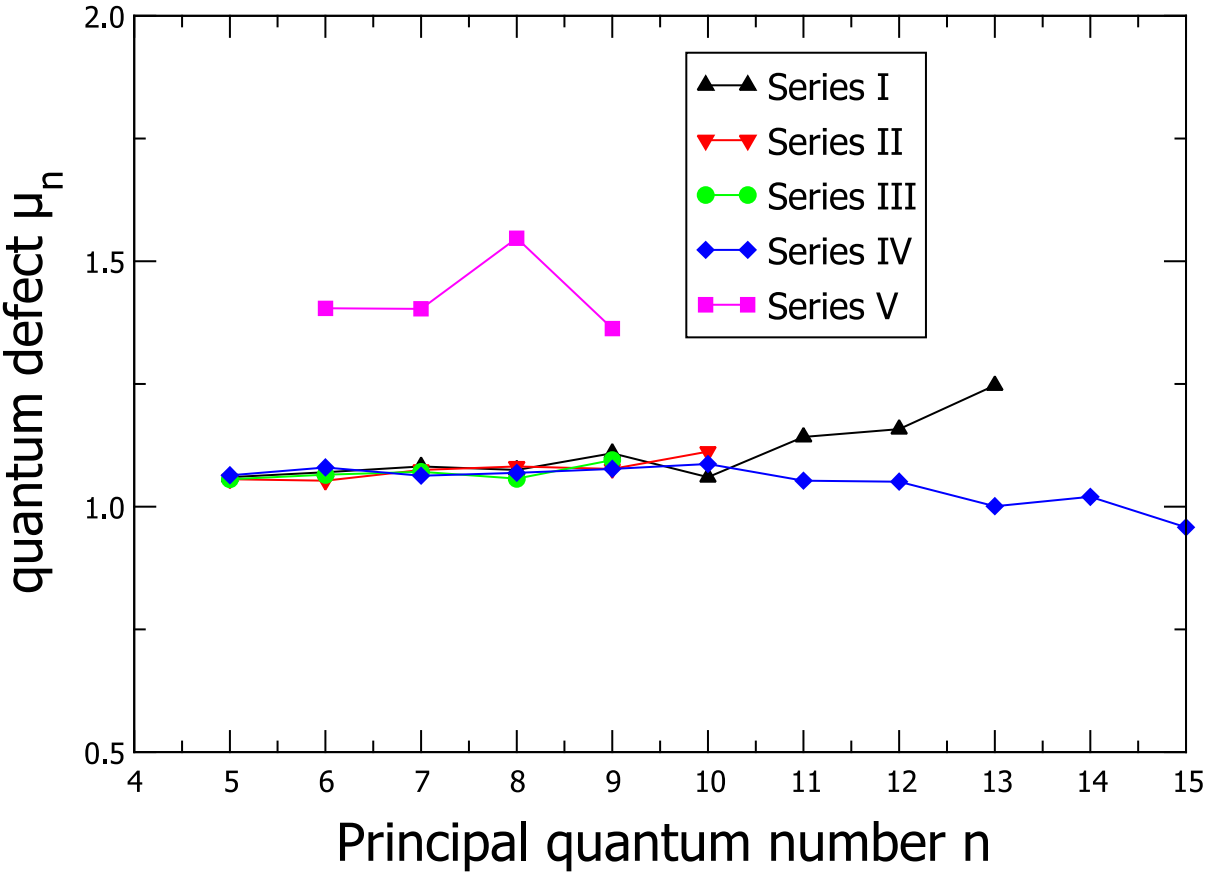

Figure 5. Quantum defect μ_n versus the principal quantum number n for the dominant resonances series found in the Zn II ALS measured spectrum for the photon energy range 24–28 eV. Table 4 gives details for resonance series labelled I, II, III, IV and V.

Table 6. Resonance energies E_n of the identified Rydberg series I, II, III, IV and V (from the large-scale DARC calculations), $J = 1/2$ odd scattering symmetry, converging to the $3d^9 4s\,^3\mathrm{D}_{3,\,2,\,1}$ triplet and the $3d^9 4s\,^1\mathrm{D}_2$ singlet states originating from the Zn^+ ground state.

	Autoionizing Zn II Rydberg resonance series energies, $J = 1/2^o$ symmetry				
	I	II	III	IV	V
	$(3d^9 4s)^3\mathrm{D}_3\,np$	$(3d^9 4s)^3\mathrm{D}_2\,np$	$(3d^9 4s)^3\mathrm{D}_1\,np$	$(3d^9 4s)^1\mathrm{D}_2\,np$	$(3d^9 4s)^3\mathrm{D}_3\,np$
n	E_n(eV)	E_n(eV)	E_n(eV)	E_n(eV)	E_n(eV)
4	–	22.044	–	22.337	22.563
5	24.149	24.583	24.141	24.747	24.780
6	25.415	25.559	25.404	25.723	25.723
7	26.101	26.220	26.082	26.345	26.345
8	26.512	26.538	26.504	26.656	26.659
9	26.780	26.849	26.773	26.909	26.910
10	26.962	26.147	26.957	27.088	27.088
⋮					
Limit	27.647	27.793	27.989	28.317	27.647

population of the ground state Zn^+, implied that the ion beam was in almost the same internal energy at both anode voltages. This explains why they did not observe any measurable differences in their PI cross-section as a function of the anode potential. Electron impact generates electronic excitation. A possible explanation for the disagreement in the resonance strengths is that the ion beam population of electronically excited states of Peart et al. (1987) was different than the population of excited states in the ion beam of the present ALS experiment.

5 CONCLUSIONS

PI cross-sections producing Zn^{2+} from Zn^+ ions were measured in the photon energy range of 17.5–90 eV with a photon energy resolution of 17 meV FWHM. All the sharp resonance features present in the spectrum (for the energy region 20–28 eV) have been analysed and identified. These resonance features we attribute to Rydberg transitions originating from the ground state Zn^+ into excited autoionizing states of the Zn^+ ion that ionize to the different $3d^9 4s\,^3\mathrm{D}_{3,\,2,\,1}$ and $3d^9 4s\,^1\mathrm{D}_2$ threshold states of Zn^{2+}. We note that

Table 7. Resonance energies E_n of the identified Rydberg series I, II, III, IV and V (from the large-scale DARC calculations), $J = 3/2$ odd scattering symmetry, converging to the $3d^9 4s\,^3\mathrm{D}_{3,\,2,\,1}$ triplet and the $3d^9 4s\,^1\mathrm{D}_2$ singlet states originating from the Zn^+ ground state.

	Autoionizing Zn II Rydberg resonance series energies, $J = 3/2^o$ symmetry				
	I	II	III	IV	V
	$(3d^9 4s)^3\mathrm{D}_3\ np$	$(3d^9 4s)^3\mathrm{D}_2\ np$	$(3d^9 4s)^3\mathrm{D}_1\ np$	$(3d^9 4s)^1\mathrm{D}_2\ np$	$(3d^9 4s)^3\mathrm{D}_3\ np$
n	E_n(eV)	E_n(eV)	E_n(eV)	E_n(eV)	E_n(eV)
4	–	22.214	21.916	22.213	22.711
5	24.148	24.311	24.447	24.503	24.745
6	25.417	25.573	24.564	25.579	25.759
7	26.101	26.243	26.233	26.330	26.330
8	26.512	26.656	26.572	26.656	26.572
9	26.780	26.858	26.853	26.868	26.817
10	26.963	26.991	–	26.991	26.991
⋮					
Limit	27.647	27.793	27.989	28.317	27.647

the DARC calculations, for resonance energies and peak heights, favour the present ALS measurements as opposed to the previous measurements from the Daresbury radiation facility (Peart et al. 1987).

The most prominent peak in the spectrum is observed at 24.141 eV in the ALS data, 24.172 eV in the Daresbury data (Peart et al. 1987) and 24.158 eV in the DARC calculations, a difference of 31 and 17 meV, respectively, see Table 5. We attribute this peak to an excited $Zn^+[3d^9 4s(^3\mathrm{D}_3)\,5p]$ autoionizing resonant state, originating from photoexcitation of the $3d^{10}4s\,^2\mathrm{S}_{1/2}$ ground state and decaying back to the state $3d^9 4s\,(^3\mathrm{D}_3)$ of Zn^{2+}. This autoionizing state is a member of the Rydberg resonance series I, see panel (a) of Fig. 2. We note that transitions from the electronically excited $3d^{10}4p\,^2\mathrm{P}^{\mathrm{o}}{}_{1/2,\,3/2}$ levels are dipole allowed to the $3d^{10}4s\,^2\mathrm{S}_{1/2}$ ground state and will not be present in the spectrum.

The cross-section below the ground state threshold at 17.964 eV does not go to zero, due to a small fraction of excited metastable states present in the Zn^+ ion beam. In addition, contributions from higher order radiation components may contaminate the photon beam. A comparison of the present results with the earlier measurements of Peart et al. (1987) reproduces all their resonant peaks but with much improved statistics. Discrepancies in the cross-sections in the low-energy regime of the spectrum we attribute to the different populations of the excited and metastable states in the ion beams of both experiments.

Interpretation of the present data was made possible using PI cross-section results determined from large-scale Dirac *R*-matrix calculations which allows for the inclusion of the interaction between closed and open channels. We traced the contributions from different initial states in the ion beam and determined the metastable fraction present in the experiment to be small, in the region of 2 per cent.

ACKNOWLEDGEMENTS

The Advanced Light Source is supported by the Director, Office of Science, Office of Basic Energy Sciences, of the US Department of Energy under Contract No. DE-AC02-05CH11231. AMC acknowledges support through Co-operative Agreement DOE-NA0002075. GH acknowledges Reyes García and Ulises Amaya for computational support, grant PAPIIT-IN-109-317 and DGAPA-PASPA sabbatical scholarship. DC acknowledges support from Sierra College and OW from the Swedish Research Council. BMMcL acknowledges support by the US National Science Foundation under the visitors programme through a grant to ITAMP at the Harvard–Smithsonian Center for Astrophysics and Queen's University Belfast through a visiting research fellowship (VRF). This research used resources of the National Energy Research Scientific Computing Centre, which is supported by the Office of Science of the US Department of Energy (DOE) under Contract No. DE-AC02-05CH11231. The computational work was performed at the National Energy Research Scientific Computing Centre in Berkeley, CA, USA and at The High Performance Computing Centre Stuttgart (HLRS) of the University of Stuttgart, Stuttgart, Germany. Grants of computing time at NERSC and HLRS are gratefully acknowledged.

REFERENCES

Andersen T., Pedersen P., Biemont E., 1997, J. Quant. Spectrosc. Radiat. Transfer, 17, 389
Ballance C. P., 2016, DARC Codes. Available at: http://connorb.freeshell.org
Ballance C. P., Berrington K. A., McLaughlin B. M., 1999, Phys. Rev. A, 60, R4217
Berkowitz J., 1979, Photoabsorption, Photoionization and Photoelectron Spectroscopy. Academic Press, New York
Bizau J.-M. et al., 2005, A&A, 439, 387
Burke P. G., 2011, R-Matrix Theory of Atomic Collisions: Application to Atomic, Molecular and Optical Processes. Springer, New York
Busso M., Gallino R., Wasserburg G. J., 1999, ARA&A, 37, 239
Cardelli J. A., Federman S. R., Lambert D. L., Theodosiou C. E., 1993, ApJ, 416, L41
Chang J. J., 1975, J. Phys. B: At. Mol. Opt. Phys., 8, 2327
Chayer P., Vennes S., Dupuis J., Kruk J. W., 2005, ApJ, 630, L169
Chen Y. Q., Nissen P. E., Zhao G., 2004, A&A, 425, 697
Clark R. E. H., Abdallah J., Jr, Mann J., 1991, ApJ, 381, 597
Covington A. M. et al., 2002, Phys. Rev. A, 66, 062710
Cowan R. D., 1981, The Theory of Atomic Structure and Spectra. Univ. California Press, Berkeley, CA
Cowan J. J., Sneden C., 2006, Nature, 440, 1151
Djeniže S., Milosavljevic V., Dimitrijevic M. S., 2003, Eur. Phys. J. D, 27, 209
Domke M., Schulz K., Remmers G., Kaindl G., Wintgen D., 1996, Phys. Rev. A, 53, 1424
Dyall K. G., Johnson C. T., Grant I. P., Parpia F., Plummer E. P., 1989, Comput. Phys. Commun., 55, 425
Eisberg R. E., Resnik R. M., 1985, Quantum Physics of Atoms, Molecules, Solids Nuclei and Particles, 2nd edn. Wiley, New York

Esteves D. A., Bilodeau R. C., Sterling N. C., Phaneuf R. A., Kilcoyne A. L. D., Red E. C., Aguilar A., 2011, Phys. Rev. A, 84, 013406
Esteves D. A., Bilodeau R. C., Phaneuf R. A., Kilcoyne A. L. D., Red E. C., Aguilar A., 2012, J. Phys. B: At. Mol. Opt. Phys., 45, 115201
Fano U., Cooper J. W., 1968, Rev. Mod. Phys., 40, 441
Frebel A., Simon J. D., Kirby E. N., 2014, ApJ, 786, 74
Ganeev R. A., Suzuki M., Yoneya S., Strelkov V. V., Kuroda H., 2016, J. Phys. B: At. Mol. Opt. Phys., 49, 055402
García-Rojas J., Madonna S., Luridiana V., Sterling N. C., Morisset C., Delgado-Inglada G., Toribio San Cipriano L., 2015, MNRAS, 452, 2606
García-Rojas J., Peña M., Flores-Durán S., Hernández-Martínez L., 2016, A&A, 586, A59
Grant I. P., 2007, Quantum Theory of Atoms and Molecules: Theory and Computation. Springer, New York
Harrison H., Schoen R. I., Cairns R. B., Schubert K. E., 1969, J. Chem. Phys., 50, 3930
Herwig F., 2005, ARA&A, 43, 435
Hinkel N. R., Timmes F., Young P. A., Pagano M. D., Turnbull M. C., 2014, AJ, 148, 54
Hollek J. K., Frebel A., Roederer I. U., Sneden C., Shetrone M., Beers T. C., Kang S., Thom C., 2011, ApJ, 742, 54
Jose J., Iliadis C., 2011, Rep. Prog. Phys., 74, 096901
Karakas A. I., van Raai M. A., Lugaro M., Sterling N. C., Dinerstein H. L., 2009, ApJ, 690, 1130
King G. C., Tronc M., Read F. H., Bradford R. C., 1977, J. Phys. B: At. Mol. Phys., 10, 2479
Kobayashi C., Nomoto K., 2009, ApJ, 707, 1466
Kramida A. E., Ralchenko Y., Reader J., NIST ASD Team 2016, NIST Atomic Spectra Database (version 5.3), National Institute of Standards, Technology, Gaithersburg, MD. Available at: http://physics.nist.gov/
Langanke K., Wiescher M., 2001, Rep. Prog. Phys., 64, 1657
Lyon I. C., Peart B., West J. B., Dolder K., 1986, J. Phys. B: At. Mol. Phys., 19, 4137
Lyon I. C., Peart B., Dolder K., West J. B., 1987, J. Phys. B: At. Mol. Phys., 20, 1471
Macaluso D. A., Aguilar A., Kilcoyne A. L. D., Red E. C., Bilodeau R. C., Phaneuf R. A., Sterling N. C., McLaughlin B. M., 2015, Phys. Rev. A, 92, 063424
McLaughlin B. M., Ballance C. P., 2012a, J. Phys. B: At. Mol. Opt. Phys., 45, 085701
McLaughlin B. M., Ballance C. P., 2012b, J. Phys. B: At. Mol. Opt. Phys., 45, 095202
McLaughlin B. M., Ballance C. P., 2015, in Resch M. M., Kovalenko Y., Fotch E., Bez W., Kobaysah H., eds, Sustained Simulated Performance 2014. Springer, Berlin, p. 173
McLaughlin B. M., Ballance C. P., Pindzola M. S., Müller A., 2015, in Nagel W. E., Kröner D. H., Resch M. M., eds, High Performance Computing in Science and Engineering '14. Springer, Berlin, p. 23
McLaughlin B. M., Ballance C. P., Pindzola M. S., Schippers S., Müller A., 2016, in Nagel W. E., Kröner D. H., Resch M. M., eds, High Performance Computing in Science and Engineering '15. Springer, Berlin, p. 51
McLaughlin B. M., Ballance C. P., Pindzola M. S., Stancil P. C., Schippers S., Müller A., 2017, in Nagel W. E., Kröner D. H., Resch M. M., eds, High Performance Computing in Science and Engineering '16. Springer, Berlin, p. 33
Mann J. B., 1983, At. Data Nucl. Data Tables, 29, 407
Mendenhall M. H., Henins A., Hudson L. T., Szabo C. I., Windover D., Cline J. P., 2017, J. Phys. B: At. Mol. Opt. Phys., 50, 115004
Mishenina T. V., Kovtyukh V. V., Soubiran C., Travaglio C., Busso M., 2002, A&A, 396, 189
Müller M., Schmidt M., Zimmermann P., 1986, Eur. Phys. Lett., 2, 359
Müller A. et al., 2014, J. Phys. B: At. Mol. Opt. Phys., 47, 215202
Müller A., Schippers S., Hellhund J., Holste K., Kilcoyne A. L. D., Phaneuf R. A., Ballance C. P., McLaughlin B. M., 2015, J. Phys. B: At. Mol. Opt. Phys., 48, 235203
Nissen P. E., Chen Y. Q., Asplund M., Pettini M., 2004, A&A, 415, 993
Nissen P. E., Akerman C., Asplund M., Fabbian D., Kerber F., Keufl H. U., Pettini M., 2007, A&A, 469, 319
Norrington P. H., Grant I. P., 1981, J. Phys. B: At. Mol. Phys., 14, L261
Parpia F., Froese-Fisher C., Grant I. P., 2006, Comput. Phys. Commun., 94, 249
Peart B., Stevenson J. G., Dolder K. T., 1973, J. Phys. B: At. Mol. Phys., 6, 146
Peart B., Lyon I. C., Dolder K. I., 1987, J. Phys. B: At. Mol. Phys., 20, 5403
Quigley L., Berrington K. A., 1996, J. Phys. B: At. Mol. Opt. Phys., 29, 4529
Quigley L., Berrington K. A., Pelan J., 1998, Comput. Phys. Commun., 114, 225
Roederer I. U., 2012, ApJ, 758, 36
Roederer I. U., Sneden C., Thompson I. B., Preston G. W., Shectman S. A., 2010, ApJ, 711, 573
Roederer I. U., Marino A. F., Sneden C., 2011, ApJ, 742, 37
Roederer I. U. et al., 2014, ApJ, 791, 32
Rogers W. T., Stefani G., Camilloni R., Dunn G. H., Mezanne A. Z., Henry R. J. W., 1982, Phys. Rev. A, 25, 737
Rydberg J. R., 1890, Phil. Mag., 29, 331
Rydberg J. R., 1893, Ann. Phys., 50, 625
Rydberg J. R., 1894, Ann. Phys., 52, 119
Seaton M. J., 1983, Rep. Prog. Phys., 46, 167
Sharpee B., Zhang Y., Williams R., Pellegrini E., Cavagnolo K., Baldwin J. A., Phillips M., Liu X.-W., 2007, ApJ, 659, 1265
Shore B. W., 1967, Rev. Mod. Phys., 39, 439
Smith V. V., Lambert D. L., 2015, ApJS, 72, 387
Sneden C., Gratton R. G., Crocker D. A., 1991, A&A, 246, 354
Stener M., Decleva P., 1997, J. Phys. B: At. Mol. Opt. Phys., 30, 4481
Sterling N. C., Dinerstein H. L., 2008, ApJS, 174, 154
Sterling N. C., Stancil P. C., 2011, A&A, 535, A117
Sterling N. C., Witthoeft M. C., 2011, A&A, 529, A147
Sterling N. C., Dinerstein H. L., Kallman T. R., 2007, ApJS, 169, 37
Sterling N. C. et al., 2009, PASA, 26, 339
Sterling N. C., Esteves D. A., Bilodeau R. C., Kilcoyne A. L. D., Red E. C., Phaneuf R. A., Aguilar A., 2011a, J. Phys. B: At. Mol. Opt. Phys., 44, 025701
Sterling N. C. et al., 2011b, Can. J. Phys., 89, 379
Sterling N. C., Porter R. L., Dinerstein H. L., 2015, ApJS, 218, 25
Sterling N. C., Dinerstein H. L., Kaplan K. F., Bautista M. A., 2016, ApJ, 819, L9
Travaglio C., Gallino R., Arnone E., Cowan J. J., Jordan F., Sneden C., 2004, ApJ, 60, 186
Tumlinson J., 2006, ApJ, 641, 1
Wallerstein G. et al., 1997, Rev. Mod. Phys., 69, 995
Yu Y. G., Li J. G., Dong C. Z., Ding X. B., Fritzsche S., Fricke B., 2007, Eur. Phys. J. D, 44, 51

This paper has been typeset from a TEX/LATEX file prepared by the author.